Energy 240 (2022) 122798

Contents lists available at ScienceDirect

Energy

journal homepage: www.elsevier.com/locate/energy

Thermo-economic analysis of a particle-based multi-tower solar power plant using unfired combined cycle for evening peak power generation

Francesco Rovense [a, b], Miguel Ángel Reyes-Belmonte [b], Manuel Romero [a], José González-Aguilar [a, *]

[a] High Temperature Processes Unit, IMDEA Energy, Avda Ramón de la Sagra, 3, 28935, Móstoles, Spain
[b] Department of Chemical, Energy and Mechanical Technology, Rey Juan Carlos University, Calle Tulipán, 28933, Móstoles, Spain

ARTICLE INFO

Article history:
Received 22 January 2021
Received in revised form
17 October 2021
Accepted 30 November 2021
Available online 1 December 2021

Keywords:
Multi-tower
Unfired combined cycle
Particle receiver
Peak power
Concentrating solar power

ABSTRACT

This work analyses a 150 MW_e multi-tower solar-only combined cycle power plant (nominal efficiency ~50%) for evening peak operation. Olivine particles are used as heat transfer fluid and thermal energy storage medium based on their suitable thermo-physical properties for high temperature operation. Technical constraints to handle hot particles lead to an integration of the power block and thermal storage system with an array of heliostat fields (with a solar receiver per field). Unitary 53.0 MW_{th} solar tower was designed to satisfy these constrains. Two electricity dispatch strategies covering the evening peak power have been analyzed. Number of solar fields and storage capacity have been optimized from thermo-economic optimization. It is concluded that the best layouts have seven solar towers and storage capacities of 2.0 GWh for the first dispatch scenario (with an electricity generation from 17:00 to 22:00) and eight solar towers with 2.5 GWh for the second one (from 17:00 to 24:00). Solar multiple is between 1.1 and 1.25. These two configurations cover 56.2% and 55.8% of the total energy demand at full power with LCOE of 14.6 c€ kWh^{-1} and 13.2 c€ kWh^{-1}. A sensitivity analysis on the components costs indicates that 11.0 c€ kWh^{-1} could be achieved.

1. Introduction

Bulk solar power production requires cost-competitive and flexible-dispatching technologies at the multi-megawatt scale. Concentrating solar power (CSP) has proven its ability to provide dispatchable electricity using low-cost thermal energy storage (TES) [1]. Ending 2019, an estimated 21 GWh of TES were indeed operating in conjunction with CSP plants worldwide, which doubled the battery storage capacity [2]. However, CSP electricity cost is at least three times higher than that of photovoltaics (PV) [3]. Increasing CSP contribution in the energy mix might proceed by means of different complementary actions; promoting hybrid solar power plants, implementing modular concepts, and developing advanced CSP technologies are three of them. The first one consists of employing hybrid PV-CSP solutions where the PV electricity is delivered to the grid during sunny hours while the more dispatchable CSP electricity provides support after sunset or during cloudy transients [4]. The design of such CSP plants for hybrid operation involves significant changes with respect to the traditional commercial plants, which are conceived to have high-capacity factors to reach the lowest levelized cost of electricity (LCOE). This new hybrid schemes might lead to low solar multiple (SM) even close to unity and store PV electricity as heat in CSP TES system. The second approach relies on using several solar collection units, each of them composed of a heliostat field and a solar tower in the case of central receiver systems (CRS), with a common and centralized TES system and a single power block [5,6]. This modular concept provides an alternative configuration in which individual optical efficiency of each solar collection unit is higher than a single system capable to supply the overall thermal power [7] and the electricity generation can start earlier by operation at partial load [8]. Finally, advances in CSP technologies address high-efficiency power cycles, new heat transfer fluids (HTF), and low-cost thermal storage, among other goals, which implementation would promote higher solar-to-electricity efficiency and lower LCOE. Thus,

* Corresponding author.
E-mail address: jose.gonzalez@imdea.org (J. González-Aguilar).

https://doi.org/10.1016/j.energy.2021.122798

Nomenclature

Acronyms

CAPEX	Capital expenditure
CC	Combined cycle
CDF	Cumulative distribution function
CF	Capacity factor
CRS	Central receiver system
CSP	Concentrating solar power
DUFB	Dense upflow fluidized bed
DS1	Dispatch strategy 1
DS2	Dispatch strategy 2
EPC	Engineering, procurement and construction costs
FP	Fluidized particles
GT	Gas turbine
HRSG	Heat recovery steam generator
HTF	Heat transfer fluid
HX	Heat exchanger
ISCC	Integrated solar combined cycle
LCOE	Levelized cost of electricity
LPT	Low pressure turbine
O&M	Operation and maintenance
OPEX	Operating expense
ORC	Organic Rankine cycle
P90	Ninetieth percentile
PTC	Parabolic trough collector
PV	Photovoltaics
sCO_2	Supercritical carbon dioxide
SM	Solar multiple
ST	Solar tower
STEC	Solar thermal electric components
TES	Thermal energy storage
TIT	Turbine inlet temperature
TOD	Time of delivery
TMY	Typical meteorological year
UF	Utilization factor

Latin Letters

a	Azimuth
e	Elevation
E	Energy
h	Hour
N	Number
r	Radius
S	Surface
y	Year
t	Time

Greek Letters

α	Conveyor heat loss coefficient
Δ	Variation
η	Efficiency

Subscripts

Cav	Cavity
HF	Heliostat field
Th	Thermal
e	Electric
Rec	Receiver

one of the main objectives for third CSP generation (or Gen3) is to make use of solar technologies adapted to 50% nominal conversion efficiency on the thermodynamic cycle [9]. However, current state-of-the-art has a conversion efficiency below that target due to the limited operation temperature [10]. Among different CSP technologies that are envisioned, higher receiver temperatures, which lead to outlet temperature of heat transfer fluids above 650 °C, will favor higher conversion efficiency by introducing supercritical Rankine cycles [11] and high temperature Brayton cycles configurations [12].

Recent studies have concluded that supercritical carbon dioxide (sCO_2) Brayton cycles can reach the 50% conversion efficiency target coupled to solar central receiver technologies [13–16]. The sCO_2 Brayton cycle operates in the supercritical region, in which the fluid exhibits liquid-like compressibility and heat transfer characteristics, while still reaching high temperatures. This enables to reduce the compressor work and increase the efficiency of the regenerator heat exchanger [17]. Despite sCO_2 Brayton cycles can reach very high efficiency (i.e. up to 58% at a turbine inlet temperature (TIT) of 800 °C [18]), the cycle operation is highly dependent on the ambient temperature, which can penalize the plant performance in desert areas [19–21]. Currently, sCO_2 Brayton cycles have not reached the industrial stage yet and despite promising findings for high temperature Brayton power cycles, 50% target efficiency under real on-sun operation conditions is still to be demonstrated. Consequently, CSP technology deployment in the short and medium term should be focused on combined cycles (CC) consisting on a topping Brayton cycle and a bottoming Rankine cycle, which in CSP leads to Integrated Solar Combined Cycle (ISCC) concepts [22–25]. Recently, Farsi and Dincer analyzed a solar-hybrid CC power plant consisting of a Brayton topping cycle with pressurized fluidized bed combustion and particles fluidized bed heat exchanger for transferring the rejected heat to the bottoming Rankine cycle [26]. They reported a 50% cycle energy efficiency and 53.8% exergy efficiency. Kang et al. presented a theoretical framework for the energy analysis of a solar-hybrid ISCC plant. The authors claimed an overall cycle efficiency from about 40% using a combined low and high-pressure Brayton cycle only, and up to 48% in a fully combined air-steam concept [27]. The use of other working fluids may increase cycle performance but with more sophisticated plant layouts. Javanshir et al. compared different CC in CSP plants and concluded that the Brayton and Organic Rankine Cycle (ORC) exhibited the highest thermal efficiency. In that configuration, helium and ethanol were used in the topping and bottoming cycles, respectively. A peak 53% thermal efficiency was reported at 1000 °C [28]. Zare et al. proposed a CC consisting of a closed Brayton cycle using helium as working fluid and two ORCs for waste heat recovery. Results shown a 56.9% power cycle thermal efficiency at 1000 °C [29]. Even though current concentrating solar thermal technologies are able to achieve this high operational temperature, it may also cause severe material issues in the solar receiver and seriously penalize heat losses by radiation.

Solid particles have been explored as HTF and thermal storage medium in CSP [30,31], since they present additional advantages with respect to commercially established molten salts, i.e. they are chemically inert and stable well above 900 °C, capable of storing energy over a greater temperature span, and are relatively cost-effective [32–34]. In this context, fluidized particles (FP) have been proposed as an alternative heat transfer fluid in dense upflow fluidized bed (DUFB) solar receivers by Flamant et al. [35,36]. In this solar receiver concept, fluidized particles (59 μm, mean diameter, d_{50} [37], and solid fraction volume in the range of 25%–35%) are

indirectly heated, when they flow upwards in vertical opaque tubes [35,36]. The DUFB solar receiver would enable to implement highly-efficient power cycles such as sCO_2 Brayton and CC in CSP plants [14]. Previous analysis reported up to 41% efficiency at nameplate capacity and 23% annual solar to electricity efficiency with a 290 MW_{th} DUFB solar receiver working at 650 °C and a subcritical Rankine cycle [38]. Steady-state preliminary results from Valentin et al. reported a 150 MW_e power block nameplate efficiency of 48.8% for a double reheat air topping cycle at 800 °C [39]. In turn, Behar et al. claimed an overall nominal efficiency (solar-to-electric efficiency) of 25.80% and from 21.16% to 24.7% for hybrid (i.e. solar-fuel) and solar-only operation modes, respectively, for a particle-based CSP plant with an 18 MW_e combined cycle [6]. The general conclusion is that DUFB-based CSP technology can achieve the requirements in terms of solar to electricity efficiency, though the cost impact and mechanical constraints of other key components like heat exchangers and particles conveyors needs careful assessment.

This work presents a thermo-economic assessment of a 150 MW_e multi-tower unfired CC solar thermal power plant operating at a TIT of 800 °C located in Ouarzazate (Morocco) and specifically designed for evening peak power generation. This particular dispatching scenario constraints the period for electricity generation (and consequently the capacity factor of the plant) to the necessary to cover the evening peak power demand, when photovoltaics is not able to provide any support either fully or partially. In fact, this scenario considers that the solar field acts as a "solar battery" that is charging during 8−14 h a day and discharging only during a limited number of peak hours. Then the thermal power outlet from the solar receivers and the power inlet to the turbine are fully decoupled. Consequently, a methodology for the optimization is required. The manuscript is organized as follows; firstly, the CSP plant, the components (TES, belt conveyors, and particles elevators) as well as the electricity dispatching scenarios are described. Then, the methodology, design procedure and figures of merit for select the best plant layout are presented. Results and discussion section addresses the solar field sizing, design, and determination of the number of solar towers. Through the analysis of parameters of merit, the most convenient layout in terms of number of solar towers and stored energy for different dispatching scenarios have been selected. A sensitivity analysis on the LCOE was then carried out, on the costs influence of belts conveyor and DUFB heat exchangers, due to the uncertainty of the costs of these components. Finally, for the two most convenient configurations, hourly electricity production and stored particles mass along the year are presented and discussed.

2. Solar combined cycle power plant description

Fig. 1 (left) shows the schematic layout of the 150.0 MW_e CSP plant, a multi-tower design with a single thermal storage subsystem and a CC power block. The number of solar fields (three units have been depicted in Fig. 1 for the sake of clarity) depends on the net power and energy requirements of the power plant. In turn, the net nominal thermal power of the unitary solar field is established by construction constraints, as it will be described later in this section. The particle transportation system is composed of belt conveyors and bucket elevators and it moves the particles between storage tanks and the base of each solar tower, and between there and the corresponding solar receiver. Each solar tower has two independent belt conveyors for hot and cold particles transportation and a bucket elevator for cold particles. Once at the solar receiver dispenser, the fluidized particles flows upward inside the absorber tubes onto which the concentrated solar flux is focused, heating the particles to the desired temperature. Hot particles flow by gravity though a thermal-insulated pipe from the solar receiver outlet towards the hot belt conveyor; no technical issues of the particle transport systems have been addressed in this work.

Under such configuration, TES system decouples solar energy collection from power cycle operation. When it is required by the dispatch strategy, hot particles leave the hot tank and transfer their heat to the working fluid of the Brayton cycle (air) by means of a particle fluidized bed-air heat exchanger. Outlet particles temperature in the solar receiver has been set to 825 °C, since it is considered the minimum threshold that the output DUFB receiver temperature must reach to obtain a TIT for adequate ISCC efficiency [6,39,40]. Dedicated design of the heat exchanger ensures limited temperature drop, thus 800 °C TIT can be ensured [40]. Olivine, a magnesium iron silicate, has been selected as particulate material due to its thermophysical properties (density, 3400 kg m^{-3}; specific heat, 1.27 kJ kg K^{-1} at 800 °C) and low cost (150−200 $/tonne) [41]. Thermal energy losses of the hot and cold particles path from the solar receiver to the heat exchangers have been accounted as 5% of the overall input thermal power from the solar receivers.

DUFB-based receiver was tested in a 100 kW_{th} prototype at the PROMES solar furnace in Odeillo (France) [35], providing design guidelines about solar peak flux, heat transfer coefficients and tubes length. These variables together with experimental data obtained from the EU project CSP2 [42] are the basis of a solar receiver model used in this work, which has been already described and applied to previous analyses [13,19,38]. Fig. 2 displays the particle receiver model, the left figure shows the cross section of the tubular panel located inside a cavity, while the right figure sketches the longitudinal section.

By technical reasons (limitation of the height of the tower to about 100 m because of the lack of availability of suitable systems to convey very high flowrates of hot particles up to the solar receiver beyond that height) and optimization of the solar receiver efficiency by using cavities that reduce the impact of high radiation thermal losses, the thermal power demanded by the 150 MW_e should be supplied with more than one solar field/receiver. Then a multi-tower concept with several solar fields should be used to feed a centralized storage system and a single turbine. From optical analysis of solar field with a tower of limited height and use of a cavity to minimize the radiation losses at the temperature of operation, it has been concluded that the unitary size per receiver should not be higher than 53 MW_{th}. Therefore, the optimization carried out is oriented to select the most appropriate number of receivers. The tube height of the receiver has been set to 7 m as trade-off length between the requisites in terms of fluidization (limited because of fluidization behavior and the trend to form slagging at higher lengths) [6,43]. Each tube has an internal diameter of 53 mm, 2.0 mm of thickness, an emissivity of 85% and an absorptivity of 90% [43]. Current literature on DUFB receivers proposes particles receiver temperature of 880 °C with peak flux of 806.0 kW m^{-2} with 80.0% thermal efficiency [6]. However, this work have considered an average and peak fluxes onto absorber panel set to 500.0 kW m^{-2} and 600.0 kW m^{-2}, respectively. Moreover, receiver model assumes an internal heat transfer coefficient of 2000 W m^{-2} K^{-1} in the solar receiver [44] and an efficiency as high as 80.0% for the solar receiver, which is a minimum value required to make it competitive with respect to the efficiency of molten salt receivers [45]. These values led to a 53 MW_{th} cavity solar receiver of 9.0 m in radius that contains 240 tubes of and separated 10.0 mm each other and an external wall temperature for the tubes.

Fig. 3 illustrates the power block scheme of the CSP plant analyzed in this contribution, while Table 1 summarizes its main characteristics; in past work [38], the methodology and the results were presented regarding the optimization of the mass flow rates

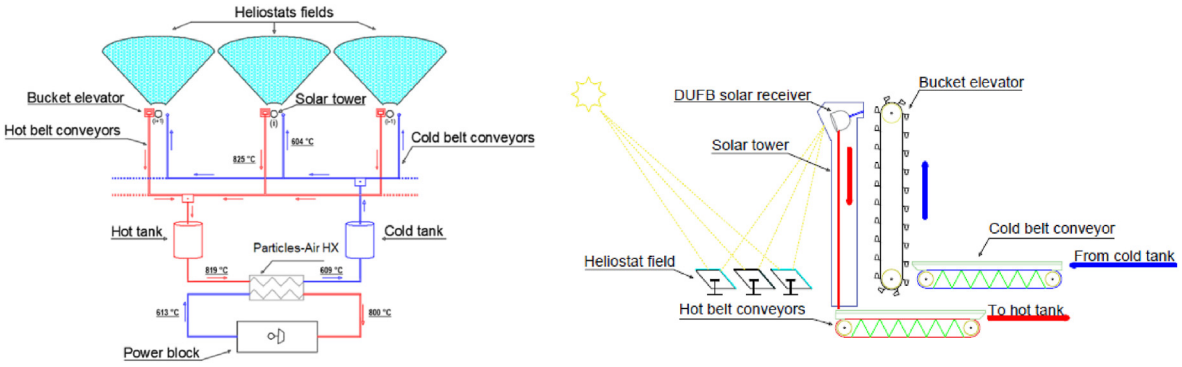

Fig. 1. (Left) Layout of the DUFB-based multi-tower CSP plant; (right) Detail layout on a solar tower.

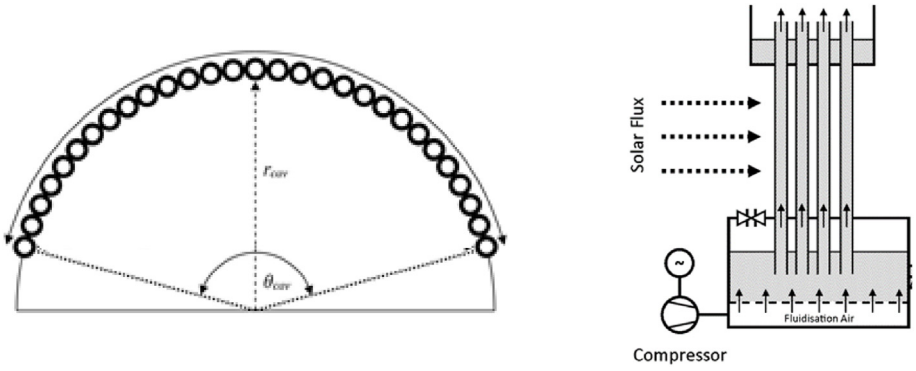

Fig. 2. Particle receiver cross section view (left); particle receiver longitudinal section view (right).

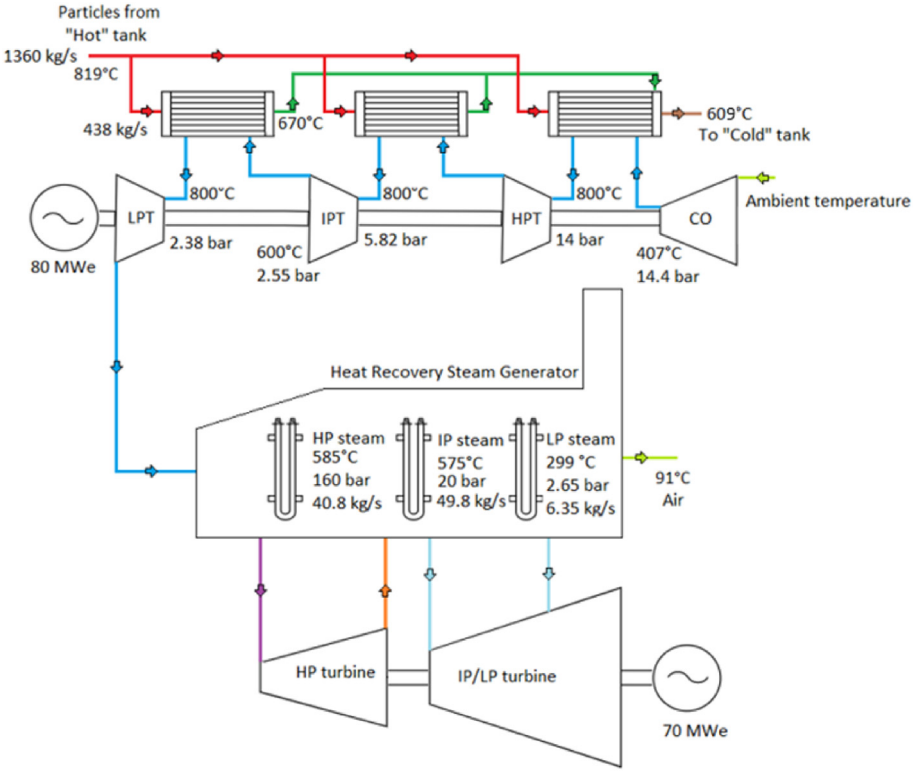

Fig. 3. Combined cycle layout of the 150.0 MWe CSP plant. Power block diagram contains pressure, temperature, and flow rates design data.

Table 1
Power block main parameters of Fig. 3.

Parameter	Value	Unit
Particle inlet temperature in particles-air-heat exchangers	819	°C
Particle inlet mass flow rate in particles-air-heat exchangers	438	kg/s
First stage particle outlet temperature from particles-air-heat exchangers	670	°C
Last stage particle outlet temperature from particles-air-heat exchangers	613	°C
HPT outlet pressure	14	bar
IPT outlet pressure	5.82	bar
LPT outlet pressure	2.38	bar
Turbine Inlet Temperature	800	°C
Turbine Outlet Temperature	600	°C
High Pressure Steam Temperature	585	°C
High Pressure Steam Pressure	160	bar
High Pressure Steam Mass Flow Rate	40.8	kg/s
Intermediate Pressure Steam Temperature	575	°C
Intermediate Pressure Steam Pressure	20	bar
Intermediate Pressure Steam Mass Flow Rate	49.8	kg/s
Low Pressure Steam Temperature	299	°C
Low Pressure Steam Pressure	2.65	bar
Low Pressure Steam Mass Flow Rate	6.35	kg/s
Outlet HRSG Air Temperature	91	°C
Compressor Outlet Air Temperature	407	°C
Compressor Outlet Air Pressure	14.6	bar

and pressure level of the power block used in this analysis. As it can be observed, the 150.0 MW_e power block consists of an 80 MW_e double reheat gas turbine (GT), a 70 MW_e three pressure level steam turbines, a heat recovery steam generator (HRSG) connecting both power cycles, and a series of air-particle fluidized bed heat exchangers. During steady-state operation, heat exchangers are fed with particles coming from the hot tank at 819 °C. Particles mass flow repartition among heat exchangers shows that air coming from the compressor can be heated up from 407 °C to 800 °C. Particles leave the heat exchanger back to the cold storage tank at 606 °C predicted by heat exchanger modelling (brown line). Double reheat GT configuration has been chosen based on its highly-regenerative nature that maximizes energy recovery from air expansion when it is divided across the high-pressure (HPT), intermediate (IPT) and low-pressure turbines (LPT). Besides it is especially appealing when high efficiency is required for moderated TIT as it is this case; the current literature indicates that reheat Brayton cycle is used with particles-based solar receiver [39] or with solar air receiver [46]. Exhaust air from the LPT feeds a 585 °C and 160.0 bar reheat Rankine cycle before leaving the HRSG at 91 °C. In this analysis, considering previous research works proving particles receiver operation [47] and particle-air heat exchanger numerical modelling, a TIT of 800 °C has been considered [48]. Based on those considerations, and on the literature data [49], net efficiency of the ISCC reached 49.4% for design conditions.

Together with the plant layout, this analysis incorporates two dispatch strategies, labelled as DS1 and DS2, which are illustrated in Fig. 4. In both dispatch strategies, electricity production starts at 17:00 and reaches full nominal power after 40 min. In DS1 (Fig. 4 left), the nominal power operation continues for 4 h and 20 min, and then it decreases to stop at 22:40 while in DS2 (Fig. 4 right) nominal power operation is 5 h and 40 min long. In both cases, desired dispatch strategies correspond to a scenario of evening and night peak demand; dispatching depends on the price of electricity in the market of the day before, but a simplification has been made in this discussion. Since solar field collection and power dispatch are decoupled through the thermal heat storage, those profiles could be easily shifted.

Connection and shut-down of the plant take place in 40 min ramp-up and ramp-down periods [50,51]. These intervals are split in two 20-min phases, in which the power block operates at lower efficiencies of 19% and 40%. Considering the targeted operation strategy, daily electrical energy production corresponds to 750 MWh_e and 950 MWh_e for DS1 and DS2, respectively.

3. Methodology

3.1. Design procedure

The design methodology and the performance analysis to carry out annual simulations of solar power plants were presented in previous works [38,49]. Both heliostat field design and receiver aperture sizing were conducted simultaneously. The solar field design of the unitary heliostat field and the flux distribution on the aperture was carried out using SolarPILOT [52] taking into account heliostat characteristics, tower height constraints, receiver peak flux inside the cavity and geometrical restrictions of the tubes. Flux maps inside the cavity and average and peak fluxes were obtained using SolTRACE open-source tool [53]. Several iterations were performed to optimize the solar field design and minimize thermal and optical losses in the receiver. The optimized solar field matrix, which was an output data from SolarPILOT, was encoded in TRNSYS tool to simulate the power plant layout. Previous works describe the TRNSYS methodology required for solar power plant simulations, both using STEC library existing models [54] and in-house encoded components for DUFB receiver and heat exchanger [40,48]. In addition, detailed control and operation strategies were defined to address storage charging and discharging operation modes as well as power block start-up and shut down, and receiver incident flux. Meteorological data of Ouarzazate (30°54′59.99″ North, 6°54′59.99″ West) with a 10-min time-step Direct Normal Irradiance (DNI) resolution from METEONORM database [55] was introduced to the weather data control toolbox in TRNSYS. Finally, data processing was performed using MATLAB scripts. The geometrical data as well the optical parameters of the pentagonal Stellio heliostats (from SBP) were considered in this analysis for their low cost and their main data are displayed in Table 2 [56]. The modelling assumptions and the boundary conditions considered are also summarized in Table 2.

3.2. Solar field design and number of solar towers

The ninetieth percentile of the DNI Cumulative Distribution Function (CDF) of the Typical Meteorological Year (TMY) data of

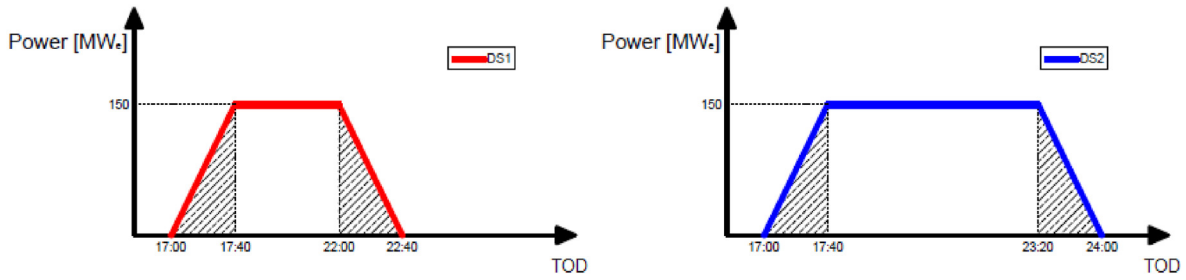

Fig. 4. Daily electric dispatch strategies as a function of the time of delivery. (Left) scenario 1, and (right) scenario 2.

Table 2
Modelling assumptions for the thermodynamic modelling.

Parameter	Assumption	Value	Unit
Heliostats			
Area	Ref. [56]	48.5	m^2
Reflectivity	Ref. [56]	93.5	%
Soiling factor	Ref. [56]	95.0	%
Beam quality	Ref. [56]	2.4	mrad
Tracking error	Ref. [56]	0.6	mrad
Solar Receiver			
Receiver active tube height	Ref. [6,43]	7.0	m
Average flux inside the cavity	Ref. [57]	500.0	kW m^{-2}
Peak flux inside the cavity	Ref. [57]	600.0	kW m^{-2}
Absorptivity of tubes	Ref. [43]	90.0	%
Emissivity of tubes	Ref. [43]	85.0	%
Tubes thickness	Ref. [57]	2.0	mm
Tubes spacing	Ref. [57]	10.0	mm
Number of tubes	Constrained	240	–
Surface cavity temperature	Ref. [44]	>900	°C
Particles inlet temperature	Constrained	609	°C
Particles outlet temperature	Ref. [57]	825	°C
Tubes internal diameter	Ref. [42]	53.0	mm
Particles mass flow	Ref. [57]	165.0	kg s^{-1}
Internal heat transfer coefficient	Ref. [27,44]	2000.0	W m^{-2} K^{-1}
Cavity radius	Constrained	9.0	m
Thermal power	Constrained	53.0	MW_{th}
Solar Field			
Tower height	Constrained	110.0	m
DNI design Point	Optimized	TMY P90	–
Receiver peak flux	Optimized	SolarPilot	–
Solar field matrix	Optimized	SolarPilot	
Fluxes maps inside the cavity	Optimized	SolTrace	
Average peak inside the cavity	Optimized	SolTrace	
Receiver thermal power	Optimized	SolarPilot	
Power block			
Gas turbine net power	Ref. [49]	80.0	MW_e
Turbine Inlet Temperature	Ref. [47]	800	°C
Steam turbine net power	Ref. [49]	70.0	MW_e
Pressure levels Steam Turbine	Ref. [49]	3	–
Air/Particles heat exchanger model	Ref. [40]	–	–
Power plant			
Number of solar towers	Optimized	–	–
TES capacity	Optimized	1.0 ÷ 3.0	GWh
Electricity production	Constrained	150.0	MW_e

Ouarzazate has been considered for the unitary solar field sizing at design point, according the definition of percentile given by Peruchena et al. [58]. Once the unitary solar field is defined, the number of solar towers (N_{ST}) is calculated as the ratio between the daily energy needed for a given dispatch scenario, E_n (with n = 1, 2), and the daily energy collected by the CSP plant (from all the solar towers). This parameter is the daily energy collected by one solar receiver $E_{Rec}(day,\ t_{start}, t_{end})$ with a correction due to heat losses in the particle conveying α_n.

$$N_{ST} = (1+\alpha_n)\frac{E_n}{E_{Rec}(day, t_{start}, t_{end})} \quad (1)$$

where t_{start} and t_{end} are the operation starting and ending time of the power plant.

The daily energy reaching a solar receiver per collecting surface area, S, is evaluated by means of the instantaneous DNI and the unitary heliostat field hourly efficiency, η_{HF}. This one is a function of the solar elevation, $e(day, t)$ and the azimuth $a(day, t)$ [59] with day = 1, …,365 and $0 \le t < 24$ h,

$$E_{Rec}(day,\ t_{start}, t_{end}) / S = \int_{t_{start}}^{t_{end}} DNI(day, t)\eta_{HF}(e, a)\mathrm{d}t \quad (2)$$

Notice that the collecting surface area and the solar field efficiency are result of the solar field optimization. It is assumed that concentrated solar energy is collected and stored around solar noon (12 h), when the solar resource is higher. Thus, eq. (2) is expressed as

$$E_{Rec}(day, \Delta t) / S = \int_{12-\Delta t/2}^{12+\Delta t/2} DNI(day, t)\eta_{HF}(e, a)\mathrm{d}t \quad (3)$$

with $\Delta t = t_{end} - t_{start}$ and $0 \le \Delta t < 24$ h. The highest limit ($\Delta t = 24\ h$) means that 24 h of the day are considered for the solar energy collection, while the lowest limit ($\Delta t = 0\ h$) means that no energy has been collected.

3.3. Power plant cost

Table 3 lists the costs used to estimate capital expenditure (CAPEX) and operating expense (OPEX) expenses. Power block cost

Table 3
Power plant components costs.

Component	Cost	Unit	Reference
Gas Turbine	23.23	M€	[62]
Steam Turbine	18.02	M€	[63–66]
Steam Recovery	23.35	M€	[64]
Conveying[a]	9.17	M€ per solar tower	[60,61]
Heliostat field	89.0 (100.0)	€ m^{-2} ($ m^{-2})	[67]
Tower	2.83	M€ per solar tower	[68]
Receiver	810.0	k€ per solar tower	[68]
Storage	17.8	€ kWh^{-1}	[69]
Heat exchangers	21.24	M€ per solar tower	[65]
OPEX	20.0	M€ MWh^{-1} y	[50]
EPC	5.0	%	[70]
Installations costs	15.0	%	[70]
Contingency	10.0	%	[70]

[a] Conveying and heat exchanger cost values range from half to double in the parametric analysis.

uniquely refers to the CC, while conveying, solar towers and heat exchangers are considered apart, since they depend on the number of ST units. Particle transportation system ("Conveying" in Table 3) includes belt conveyors and bucket elevators. Two types of belt conveyors, with a slope of 0.1 m and two different length modules (0.4 m and 1.6 m) have been considered. Due to the multi-tower solar plant arrangement, each ST requires two belts that connect the TES system to the power plant (800 m length belt) and one secondary line with 200 m length that conveys particles from the main path to the bucket elevator. Considering that each path requires two-tracks to separate hot and cold particles, transportation costs are twice. Unitary cost of 120 \$ m^{-1} (106.8 € m^{-1}) for the secondary path (0.4 m width, 200 m length) and 180 \$ m^{-1} (160.2 € m^{-1}) for the main path (1.6 m width, 800 m length) can be found in mining-related literature [60,61]. Therefore, the cost of each track is 4.48 M€ per solar. Moreover, bucket elevator cost is estimated in 200 k€ including installation and transportation costs from mining projects experiences. Consequently, the unit cost for the conveying is 9.17 M€ per solar tower, since this has two tracks for the hot and cold particle streams and a bucket elevator. TES costs is expressed in terms of stored energy, while the OPEX costs are referred to the electricity energy produced per year.

Finally, capacity factor (CF), utilization factor (UF), solar-to-electricity efficiency (η) and the levelized cost of electricity (LCOE) have been used to optimize the CSP plant. The difference between the CF and the UF is related to the operational hours; first parameter considers the ratio of the energy production and theoretical highest annual production (corresponding to 8760 h at full power) while the second, the ratio of the yearly energy production and dispatchable energy related to DS1 and DS2. The solar-to-electricity efficiency indicates the capability of the plant to convert the available solar energy in electricity. The parameters related to the LCOE of the discount rate (5%) and plant lifetime (30 years) have been considered [68].

4. Results and discussion

4.1. Solar field unit

Fig. 5 shows the CDF of the DNI (10-min data) and the daily energy received by the solar field per square meter in red and blue solid lines, respectively. The ninetieth percentile for the DNI curve corresponds to 907.0 W m^{-2} that has been taken as the design point. Similarly, the ninetieth percentile for the daily energy

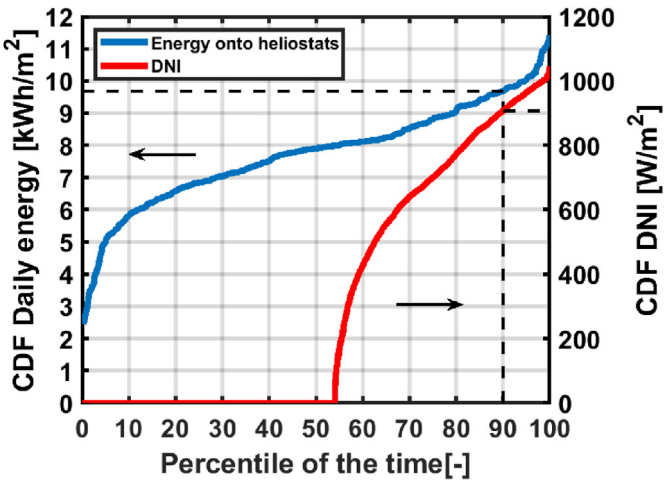

Fig. 5. CDF of daily energy incident into receiver and DNI.

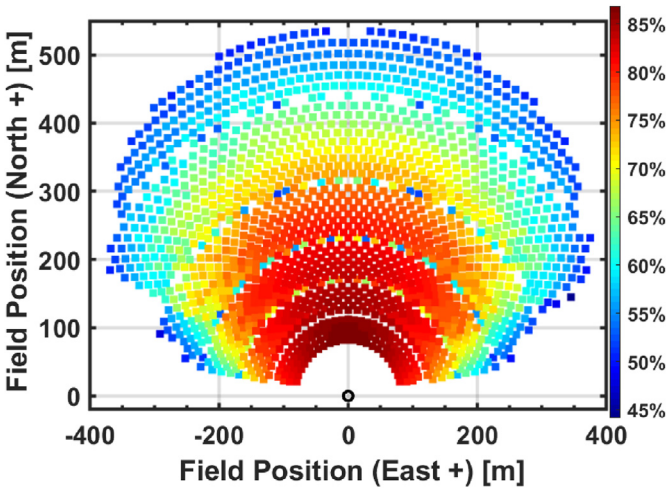

Fig. 6. Solar field layout and efficiency.

Table 4
Main characteristics of the unitary heliostat field designed with SolarPILOT.

Component	Value	Unit
Heliostat area	83,971	m^2
Number of heliostats	1731	–
Power incident on field	75.6	MW_{th}
Shadowing and Cosine efficiency	92.7	%
Reflection efficiency	88.0	%
Blocking efficiency	99.1	%
Image intercept efficiency	88.8	%
Solar field optical efficiency	69.6	%

reaching the unitary heliostats field corresponds to 9.67 kWh m^{-2}.

Fig. 6 sketches the unitary heliostat field layout obtained after optimization with SolarPILOT. Table 4 summarizes the results from the design of this unitary solar field. As it can be observed, the average optical efficiency at design point reaches 69.6% while the thermal efficiency of the receiver reaches a value of 79.4%, very close to 80.0%.

4.2. Number of solar towers

Fig. 7 shows the CDF of the daily energy reaching the DUFB solar receiver aperture versus the percentile of the days for different collecting energy time. Violet solid line labelled by $\Delta t = 24$ h represents the CDF of the highest daily energy available that a solar receiver can collect. The plot points out that the DNI selected in the design point and defined by criterion of the ninetieth percentile of days (black dashed line) enables to collect from 237.55 MWh in 8-h operation of the solar tower up to 448.32 MWh in 24-h.

Fig. 8 displays the numbers of solar towers, calculated from Eq. (3), as a function of the CDF of the days for the dispatch scenarios 1 and 2. As expected, the lower the daily energy collected per ST, the higher the number of ST will be. In particular, around 21 ST are needed in both scenarios when the solar fields operates 6 h. Enlarging the collection time, the number of ST is reduced and reaches 7.9 for scenario one and 8.3 for scenario two for $\Delta t = 12$ h and 7.2 for scenario one and 7.5 for scenario two, when total available energy is collected.

Cases $\Delta t = 12$ h and $\Delta t = 24$ h show very similar results for both dispatch strategies, since main difference are night hours; also the number of ST is similar, considering the ninetieth percentile.

The SM is defined as the ratio between the thermal power

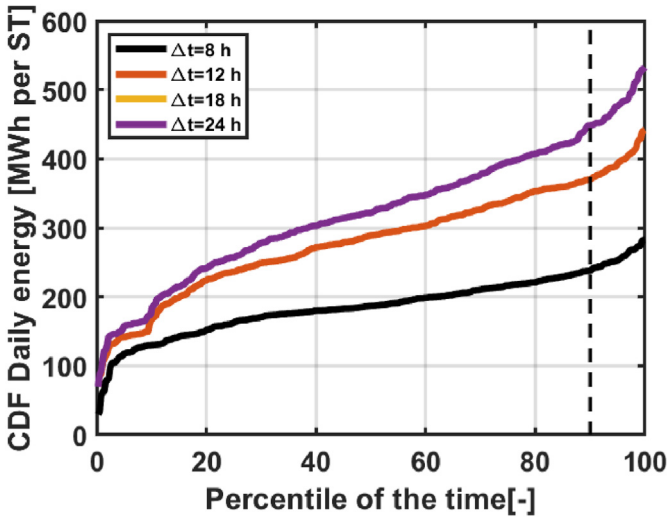

Fig. 7. Daily collected energy in the receiver for a single solar tower.

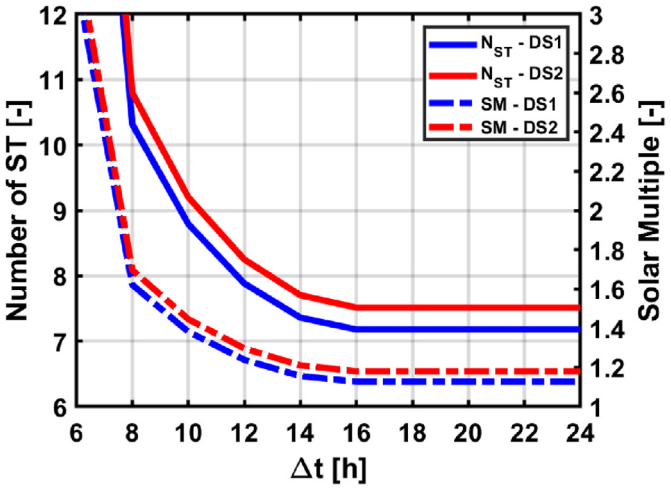

Fig. 9. Number of solar towers and solar multiple vs. operation time of solar fields.

collected from all the solar towers and the thermal power required by the power block for both dispatch strategies. Fig. 9 shows the number of solar towers (solid lines) and the respective SM (dashed lines) trends versus the Δt from 6 h to 24 h; the blue trends display the dispatching scenario 1 while the red the ones of DS2. The right y-axis indicates the SM and refers to the dashed lines, while the left y-axis indicates the number of ST and refers to the solid lines. It can be noticed that for $\Delta t > 12$ h, the N_{st} remains between 7 and 8 and the corresponding SM is between 1.1 and 1.25. Based on previous discussion, annual simulations of the proposed solar power plant were performed considering both dispatch strategies and taking into account seven and eight solar towers. For each scenario, six different TES capacities were considered, what results into twenty-four different simulations.

4.3. Electricity production

Based on the energy required by the dispatch strategy (described in the previous section), 2.0 GWh TES capacity was considered as the starting point for the sensitivity analysis (which corresponds to an amount close to 30,000 tonne of particles). In addition, the available literature data report for PTC and molten salt towers the same amount of stored energy [70]. A sensitivity analysis on the storage capacity has been conducted in order to investigate on the plant performance implications.

Table 5 gathers different capacity scenarios and the equivalent amount of particles in terms of storage capacity (in GWh) and the corresponding operational hours. Parametric analysis was conducted for stored energy increments of 0.5 GWh for both preferred configurations (seven and eight ST). As it can be noticed, for a given dispatch scenario and solar towers number, there is a maximum in the operational hours of the power block as the collected solar energy cannot further increase by enlarging storage tanks capacity. In all cases, TES system was considered fully insulated and no thermal losses were accounted .

Table 6 shows energy production results, considering the part load operations of the power block, for the different scenarios. As it can be observed, increasing the energy capacity of the storage tanks (from 1.0 to 2.5 GWh) is translated into an increase of the electricity produced by the power block. However, the expansion of the TES above 2.5 GWh does not make any difference in the electricity production in any case, since thermal energy harvested from the solar fields is not enough. In fact, enlarging tanks capacity up to 3.0 GWh makes no difference if either the number of ST is increased, or the dispatch strategy change. For the smallest tank capacities (1.0 GWh and 1.5 GWh) the power block annual production is not affected by the dispatch strategy but a small increase is observed when moving from seven to eight ST. Main differences in the energy production and dispatch strategy are found as the TES increases in the range of 2.0 and 2.5 GWh.

4.4. Capacity and Utilization factors

Fig. 10 displays the capacity factor and the utilization factor of CSP plants with 7 and 8 solar towers as a function of the energy

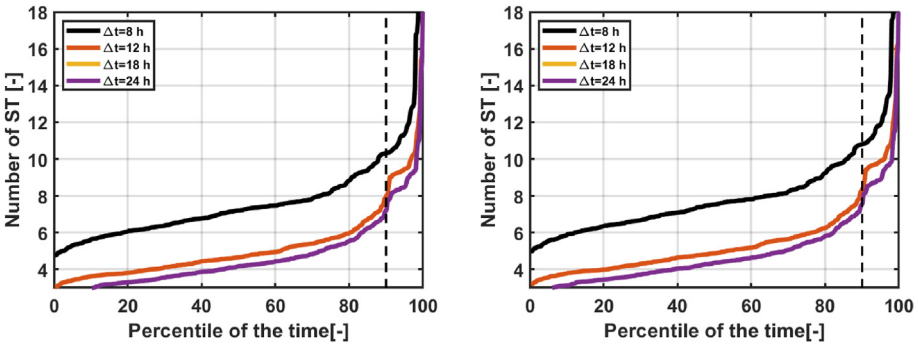

Fig. 8. CDF number of solar towers. (Left) Dispatch scenario 1; (right) dispatch scenario 2.

Table 5
Amount of particles corresponding to energy stored and operational power plant hours.

Energy stored [GWh]	Operational hours DS1 − 7 ST [h]	Operational hours DS1 − 8 ST [h]	Operational hours DS2 − 7 ST [h]	Operational hours DS2 − 8 ST [h]	Required particle mass [10^3 tonne]
1.0	949.7	954.5	949.7	954.5	14,062
1.5	1439.7	1482.3	1439.7	1482.3	21,093
2.0	1769.5	1856.7	1794.3	1888.5	28,124
2.5	1777.5	1865.2	2004.8	2149.5	35,155
3.0	1777.5	1865.2	2010.0	2149.5	42,186

Table 6
Electricity energy production [GWh].

Stored Energy [GWh]	DS1		DS2	
	Seven ST	Eight ST	Seven ST	Eight ST
1.0	115.075	115.800	115.075	115.800
1.5	188.058	194.975	188.575	194.975
2.0	238.050	251.125	241.775	255.900
2.5	239.250	252.400	274.125	295.050
3.0	239.250	252.400	274.125	295.050

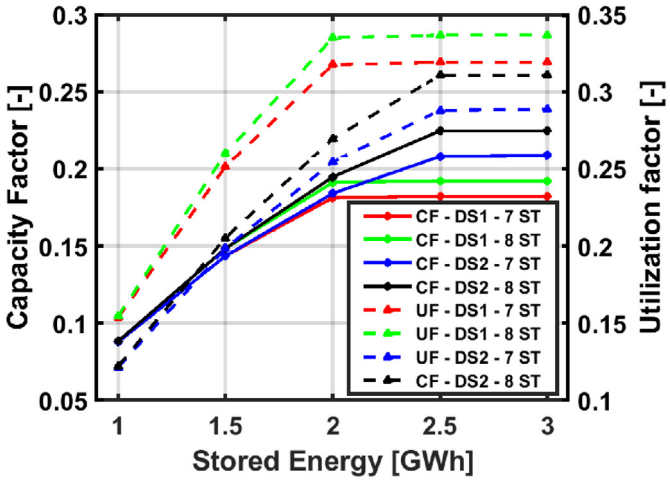

Fig. 10. Capacity and Utilization factors results for all ST configurations.

storage capacity (GWh) for both dispatch scenarios. Regarding the dispatch strategy 2, the highest CF are 20.86% and 22.45% using seven and eight ST, respectively. In turn, the highest UF is 33.48% for dispatch scenario DS1 when using eight ST and 2.0 GWh storage capacity. As it can be observed for dispatch DS2, the highest UF appears for 2.5 and 3.0 GWh storage capacity. Simulation results on eight ST show a maximum UF value of 31.06%, while that on seven ST configuration illustrates that the higher UF is 28.86%. Utilization factor confirms, regarding the energy storage, the most suitable configurations are 2.0 GWh for DS1 and 2.5 GWh for DS2.

The trend observed for the dispatching DS1 shows that the highest CF value of 18.21% is reached for the 2.0 GWh storage capacity with no benefit when increasing it up neither to 2.5 nor 3.0 GWh. With eight ST layout, an increase in CF is observed up to 19.11% with no improvement beyond 2.0 GWh storage capacity.

It must be pointed out that for this index (CF), it has been considered the electricity production of the power block along the year (8760 h) but not the limitations due the plant dispatch strategies. Therefore, the increasing of ST numbers has a direct impact into the increase of the plant capacity factor. Regarding energy utilization factor, 2.0 GWh is the optimum storage capacity for DS1 strategy while 2.5 GWh is the optimum for DS2 strategy.

4.5. Solar-to-electricity efficiency

As it can be observed in Fig. 11, the highest conversion efficiency is 17.38% for scenario two with seven ST and a storage capacity between 2.5 GWh and 3.0 GWh. Using eight ST leads to a lower maximum efficiency equals to 16.37% for the highest capacity values. For dispatching DS1, a maximum η of 15.09% is observed for seven ST configuration and 2.0 GWh storage capacity while it drops to 13.93% for eight ST layout. Solar-to-electricity efficiency indicates that seven ST and 2.5 GWh capacity is the optimum configuration for DS2 dispatch strategy while eight ST with 2.0 GWh capacity is the most suitable one for DS1 dispatch scenario.

Efficiency is directly related to the thermal storage capacity, which is mainly established by the dispatch scenario as shown in section 4.3. Thus the longest dispatch scenario, that is, DS2, provides the highest solar-to-electricity efficiency. This result suggests that other dispatch scenarios that include early-morning as well as evening peak demands might lead to higher efficiency (and in turn lower LCOE).

4.6. Levelized cost of electricity

LCOE versus the storage capacity has been plotted in Fig. 12. The lowest LCOE is 13.2 c€ kWh^{-1} for the dispatch scenario 2 with 2.5 GWh storage capacity and an arrangement of eight solar towers. Regarding DS1, the minimum LCOE is 14.6 c€ kWh^{-1} with 2.0 GWh storage capacity and seven ST. LCOE comparison between arrangements composed of seven and eight ST for each scenario points out small differences. For instance, 14.6 c€ kWh^{-1} and 15.0 c€ kWh^{-1} for seven and eight ST, respectively, and 2.0 GWh storage capacity in scenario one. This happens because the dispatch

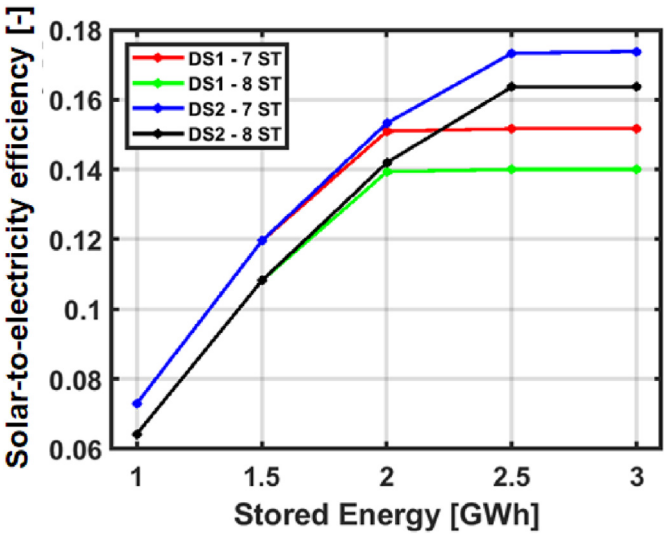

Fig. 11. Solar-to-electricity efficiency vs. thermal energy storage capacity.

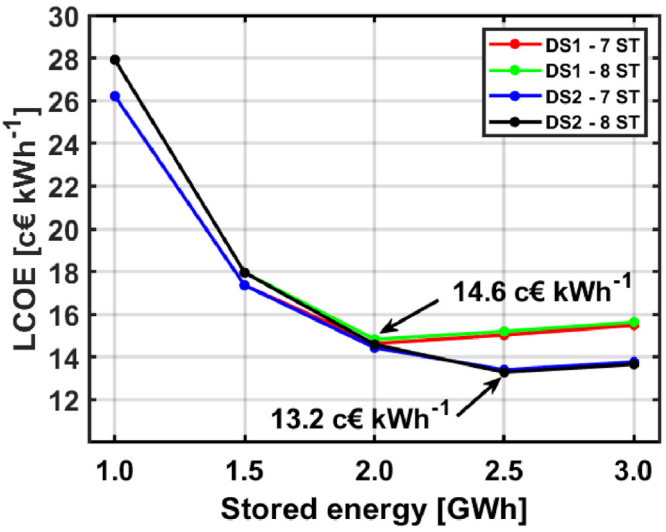

Fig. 12. LCOE vs. storage capacity for DS1 and DS2 and arrangements of seven and eight solar towers.

scenarios constraint the maximum energy produced, which are covered for both configurations and penalties due to the additional ST cost has not a significant impact on the LCOE. As shown in the previous section, the set number of delivery hours limits the CF and UF values; the increase in storage size (over 2.0 GWh for DS1 and 2.5 GWh for DS2) does not allow to increase the energy production. Consequently, the LCOE reaches a minimum value for 2.0 GWh (for DS1) and 2.5 GWh (for DS2), which corresponds to the best CF of 18.21% and 22.45%, after which it increases again. This figure points out that increasing solar plant capacity beyond 2.0 GWh (for DS1) and 2.5 GWh (for DS2) will have a negative impact in plant LCOE as extra stored energy will not be sufficient to compensate the larger plant sizing for the given dispatch scenario.

CAPEX of several CSP components such as those of the particles transportation system (belts conveyors and bucket elevators) and particles-air heat exchangers exhibits important uncertainties. The following analysis is necessary to understand how these costs can influence the cost of electricity; therefore, a sensitivity analysis of these costs on the LCOE has performed for the best cases at each dispatch strategy. This study assumes that these costs could double the reference base CAPEX.

Fig. 13 results of the sensitivity analysis for the case of seven ST − 2.0 GWh TES (Fig. 13, left) and eight ST − 2.5 GWh TES (Fig. 13, right), respectively. Fig. 13, left, shows that doubling the cost of heat exchangers, the LCOE increases up to 15.6 c€ kWh^{-1}, while reducing the costs in one half decreases the LCOE to 13.9 c€ kWh^{-1}. As it is depicted, doubling the transportation cost, the LCOE reaches 17.3 c€ kWh^{-1}, while halving them, the LCOE decreases to 12.2 c€ kWh^{-1}. As for the previous case, in Fig. 13 on the right, has been displayed the sensitivity analysis for the case powered by eight ST. If the particle transportation costs doubles, the LCOE could grow up to 15.8 c€ kWh^{-1}, while if decreases could be of 11.0 c€ kWh^{-1}, with a subsequent reduction of 2.2 c€ kWh^{-1}. On the contrary, the effect of the heat exchangers variation is lower, in fact, by increasing the CAPEX, the LCOE could be of 14.1 c€ kWh^{-1}, while decreasing could be possible to reach only 12.7 c€ kWh^{-1}.

The LCOE analysis made it possible to choose the best system configuration and enable to compare this technology with others currently existing. The best configuration of eight solar towers and 2.5 GWh of storage reaches a LCOE of 13.2 c€ kWh^{-1}, while the CAPEX reduction of the conveying system allows a LCOE of 11.0 c€ kWh^{-1}. These costs show that the technology, despite the highly-constraint dispatch scenarios analyzed, are in-line with the cost predictions, between 10.0 and 13.0 c$ kWh^{-1}, from other particles receiver research works [71] and project perspectives in North Africa [72].

4.7. Dispatch strategy

Fig. 14 displays the electrical energy output along the year for the CSP plants with lowest LCOE for DS1 and DS2. As it can be observed, nameplate power production of 150.0 MW_e is achieved and secured for the most part of the year; from day 66−271 in DS1 and from day 68 to day 272 in DS2, which represents 56.16% and 55.8% of total days. It can be noticed that during winter and fall there is not enough thermal energy harvested from the solar field and nameplate capacity can only be satisfied for a couple of hours.

Fig. 15 shows the amount of stored particles as a function of time; the day of the year is on the x-axis and the hour of the day is on the y-axis. The color bar on the right shows the number of stored particles (in 10^3 tonne) and change from dark blue (when no particles in the storage) to dark red (for a totally full storage). As it can be observed, the hot tank reaches it maximum capacity before electricity supply starts (at 17:00) between days 60 and 280. Moreover, the hot tank is not completely emptied in summer, although the remaining amount of particles is not enough to consider an extension of the electricity production.

5. Conclusions

In this work, the thermo-economic analysis of a multi-tower integrated solar-only combined cycle power plant has been carried out. Two cases for evening peak electricity dispatch have been considered. The use of different unitary solar fields (powering the

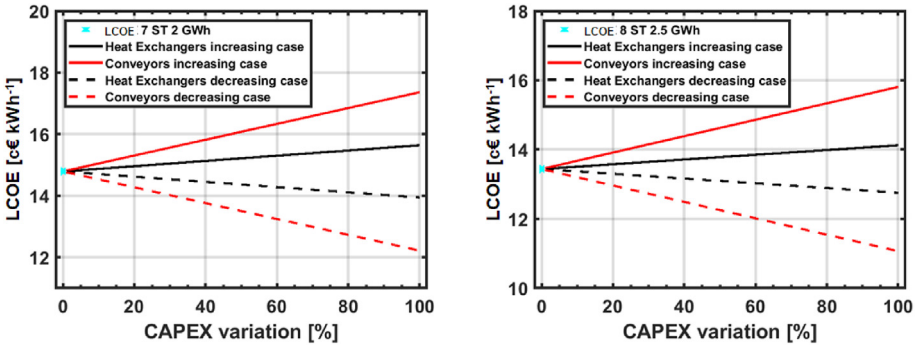

Fig. 13. Sensitivity analysis on LCOE. (Left) 7 ST − 2.0 GWh TES; (right) 8 ST − 2.5 GWh TES.

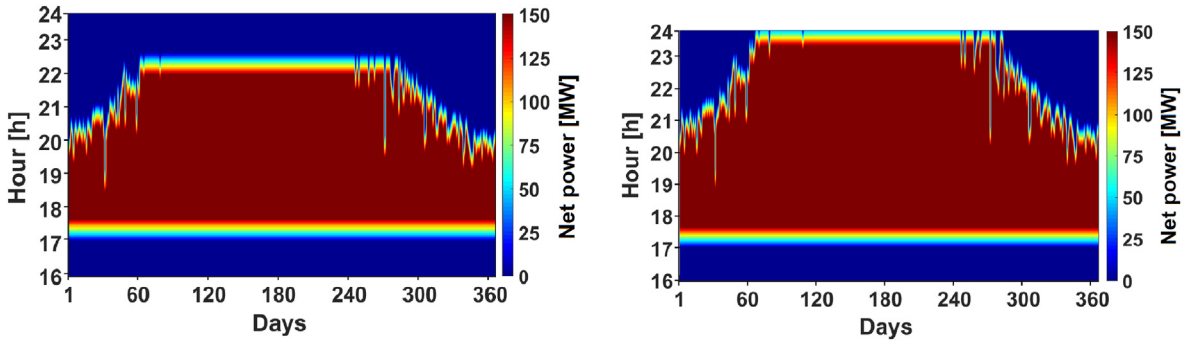

Fig. 14. Net electricity production along the year for the optimum CSP plants in each dispatching scenario. (Left) DS1, seven ST, 2.0 GWh; (Right) DS2, eight ST, 2.5 GWh.

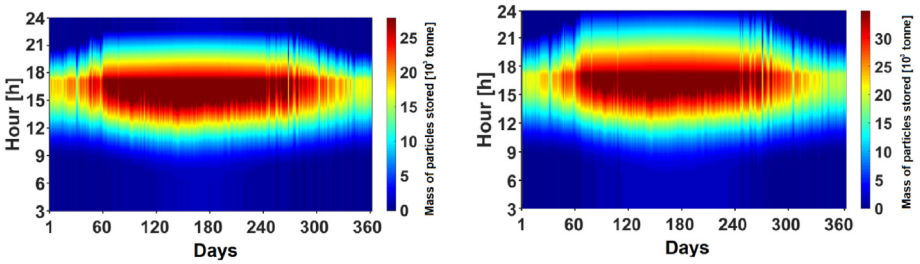

Fig. 15. Amount of particle stored in the hot silo along the year for the optimum CSP plant size in each dispatch scenario. (Left) DS1, seven ST, 2.0 GWh; (right) DS2, eight ST, 2.5 GWh.

150.0 MW_e CC), with a solar cavity receiver capacity of 53.0 MW_{th}, is based on technical constraints imposed by the DUFB technology (maximum tube length and peak flux onto the absorber), particles conveyors vertical uplift, and the reduction of cavity thermal losses at high operating temperatures. Considering the two analyzed dispatch scenarios, the solar energy harvesting, and the electricity production are decoupled and a methodology for storage capacity sizing and number of solar towers determination has been proposed. That methodology has been based on the selection of the 90th percentile of the Cumulative Distribution Function of the DNI and of the hours of solar energy collection; it allowed to choose the number of solar towers and SM minimizing the LCOE and the stored energy, and at the same time fulfil the electricity demand imposed by the different dispatch scenarios. The use of figures of merit (UF, CF, and η) related to the energy analysis allowed for optimum storage size selection.

Seven and eight solar towers that correspond to a SM of 1.1 and 1.25 were determined for each dispatch scenario as the optimum solution. The LCOE analysis for the 150.0 MW_e solar-only CC CSP plant shows that the most economic configuration for the dispatch cases given are seven solar towers with 2.0 GWh of storage for DS1, and eight solar towers with 2.5 GWh for DS2, with a LCOE of 14.6 c€ kWh^{-1} (CF = 18.21%) and 13.2 c€ kWh^{-1} (CF = 22.45%), respectively. In these configurations and considering the dispatch strategy, the power block is able to cover 56.16% of the total time of delivery for the DS1 and 55.8% for the DS2 at full power rate. The analysis suggest that additional LCOE reduction might be expected in dispatch scenarios that include evening as well as early-morning electricity peak demands.

A sensitivity analysis on costs of the particle transport system and the particle-air heat exchanger points out that LCOE below 11.0 c€ kWh^{-1} if the first is uniquely considered and the contribution of the particle transportation is three times higher than that of the heat exchanger. This analysis suggests that multi-tower configuration is highly affected by DUFB-based CSP due to the strong penalties on costs though particle transport subsystems.

Credit author statement

Francesco Rovense: Methodology, Investigation, Software, Validation, Writing, Original draft. **Miguel Ángel Reyes-Belmonte**: Methodology, Investigation, Writing, Software, Validation, Review & editing. **Manuel Romero**: Funding acquisition, Conceptualization, Investigation, Resources, Project administration, Writing, Review & editing. **José González-Aguilar**: Funding acquisition, Investigation, Conceptualization, Validation, Resources, Writing, Review & editing.

Declaration of competing interest

The authors declare that they have no known competing financial interests or personal relationships that could have appeared to influence the work reported in this paper.

Acknowledgements

This project has received funding from the European Union's Horizon 2020 research and innovation programme under grant agreement No. 727762 (Next-CSP). The authors wish to thank "Comunidad de Madrid" for its support to the ACES2030-CM project (S2018/EMT-4319) through the Program of R&D activities between research groups in Technologies 2018, co-financed by European Structural Funds.

References

[1] Flueckiger SM, Iverson BD, Garimella SV, Pacheco JE. System-level simulation of a solar power tower plant with thermocline thermal energy storage. Appl Energy 2014;113:86–96. https://doi.org/10.1016/j.apenergy.2013.07.004.
[2] Renewables REN21. Global status report. 2020. 2020.
[3] IRENA. The power to change: solar and wind cost reduction potential to 2025. 2016.

[4] Cocco D, Migliari L, Petrollese M. A hybrid CSP-CPV system for improving the dispatchability of solar power plants. Energy Convers Manag 2016;114:312–23. https://doi.org/10.1016/j.enconman.2016.02.015.

[5] Benmakhlouf Y, Guédez R, Wallmander J, Laumert B. A methodology to assess the market potential and identify most promising business cases for small scale CSP plants with thermal energy storage. AIP Conf Proc 2019;2126:130001. https://doi.org/10.1063/1.5117643.

[6] Behar O, Grange B, Flamant G. Design and performance of a modular combined cycle solar power plant using the fluidized particle solar receiver technology. Energy Convers Manag 2020;220:113108. https://doi.org/10.1016/j.enconman.2020.113108.

[7] Crespo L, Ramos F. Making central receiver plants modular, more efficient and scalable. AIP Conference Proceedings 2020;2303:030010. https://doi.org/10.1063/5.0028916.

[8] Lim JH, Chinnici A, Dally B, Nathan G. Assessing the techno-economics of modular hybrid solar thermal systems. AIP Conf Proc 2017;1850:110007. https://doi.org/10.1063/1.4984481.

[9] Mehos M, Turchi C, Vidal J, Wagner M, Ma Z, Ho C, et al. Concentrating Solar Power Gen3 Demonstration Roadmap. Nrel/Tp-5500-67464 2017:1–140. https://doi.org/10.2172/1338899.

[10] Dunham MT, Iverson BD. High-efficiency thermodynamic power cycles for concentrated solar power systems. Renew Sustain Energy Rev 2014;30:758–70. https://doi.org/10.1016/j.rser.2013.11.010.

[11] Tsiklauri G, Talbert R, Schmitt B, Filippov G, Bogoyavlensky R, Grishanin E. Supercritical steam cycle for nuclear power plant. Nucl Eng Des 2005;235:1651–64. https://doi.org/10.1016/j.nucengdes.2004.11.016.

[12] Kusterer K, Braun R, Moritz N, Lin G, Bohn D. Helium brayton cycles with solar central receivers: thermodynamic and design considerations. American Society of Mechanical Engineers Digital Collection Proc. ASME Turbo Expo 2012;6:271–9. https://doi.org/10.1115/GT2012-68407. 6.

[13] Iverson BD, Conboy TM, Pasch JJ, Kruizenga AM. Supercritical CO2 Brayton cycles for solar-thermal energy. Appl Energy 2013;111:957–70. https://doi.org/10.1016/j.apenergy.2013.06.020.

[14] Reyes-Belmonte MA, Sebastián A, González-Aguilar J, Romero M. Performance comparison of different thermodynamic cycles for an innovative central receiver solar power plant. AIP Conf Proc 2017;1850:160024. https://doi.org/10.1063/1.4984558.

[15] Binotti M, Astolfi M, Campanari S, Manzolini G, Silva P. Preliminary assessment of sCO2 cycles for power generation in CSP solar tower plants. Appl Energy 2017;204:1007–17. https://doi.org/10.1016/j.apenergy.2017.05.121.

[16] Sorbet FJ, De Mendoza MH, García-Barberena J. Performance evaluation of CSP power tower plants schemes using supercritical carbon dioxide Brayton power cycle. AIP Conf Proc 2019;2126:030056. https://doi.org/10.1063/1.5117568.

[17] Angelino G. Perspectives for the liquid phase compression gas turbine. J Eng Gas Turbines Power 1967;89:229–36. https://doi.org/10.1115/1.3616657.

[18] Zhu H, Wang K, He Y. Thermodynamic analysis and comparison for different direct-heated supercritical CO2 Brayton cycles integrated into a solar thermal power tower system. Energy 2017;140:144–57. https://doi.org/10.1016/j.energy.2017.08.067.

[19] Dyreby J, Klein S, Nellis G, Reindl D. Design considerations for supercritical carbon dioxide brayton cycles with recompression. J Eng Gas Turbines Power 2014;136:101701. https://doi.org/10.1115/1.4027936.

[20] Reyes-Belmonte MA, Sebastián A, Romero M, González-Aguilar J. Optimization of a recompression supercritical carbon dioxide cycle for an innovative central receiver solar power plant. Energy 2016;112:17–27. https://doi.org/10.1016/j.energy.2016.06.013.

[21] Chen R, Romero M, González-Aguilar J, Rovense F, Rao Z, Liao S. Design and off-design performance comparison of supercritical carbon dioxide Brayton cycles for particle-based high temperature concentrating solar power plants. Energy Convers Manag 2021;232:113870. https://doi.org/10.1016/j.enconman.2021.113870.

[22] Schwarzbözl P, Buck R, Sugarmen C, Ring A, Marcos Crespo MJ, Altwegg P, et al. Solar gas turbine systems: design, cost and perspectives. Sol Energy 2006;80:1231–40. https://doi.org/10.1016/j.solener.2005.09.007.

[23] Buck R, Giuliano S, Uhlig R. Central tower systems using the Brayton cycle. In: Advances in concentrating solar thermal research and technology; 2017. p. 353–82. https://doi.org/10.1016/B978-0-08-100516-3.00016-2.

[24] Madhlopa A. Design and testing of solar gas turbines in principles of solar gas turbines for electricity generation. Springer International Publishing; 2018. p. 163–204. https://doi.org/10.1007/978-3-319-68388-1_7.

[25] Behar O, Khellaf A, Mohammedi K, Ait-Kaci S. A review of integrated solar combined cycle system (ISCCS) with a parabolic trough technology. Renew Sustain Energy Rev 2014;39:223–50. https://doi.org/10.1016/j.rser.2015.12.092.

[26] Farsi A, Dincer I. Thermodynamic assessment of a hybrid particle-based concentrated solar power plant using fluidized bed heat exchanger. Sol Energy 2019;179:236–48. https://doi.org/10.1016/j.solener.2018.12.046.

[27] Kang Q, Dewil R, Degrève J, Baeyens J, Zhang H. Energy analysis of a particle suspension solar combined cycle power plant. Energy Convers Manag 2018;163:292–303. https://doi.org/10.1016/j.enconman.2018.02.067.

[28] Javanshir A, Sarunac N, Razzaghpanah Z. Thermodynamic analysis and optimization of single and combined power cycles for concentrated solar power applications. Energy 2018;157:65–75. https://doi.org/10.1016/j.energy.2018.05.137.

[29] Zare V, Hasanzadeh M. Energy and exergy analysis of a closed Brayton cycle-based combined cycle for solar power tower plants. Energy Convers Manag 2016;128:227–37. https://doi.org/10.1016/j.enconman.2016.09.080.

[30] Ho CH. A review of high-temperature particle receivers for concetrating solar power. Appl Therm Eng 2016;109:958–69. https://doi.org/10.1016/j.applthermaleng.2016.04.103.

[31] Falcone PK, Noring JE, Hruby JM. Assessment of a solid particle receiver for a high temperature solar central receiver system, SAND8vols. 5–820; 1985. https://doi.org/10.2172/6023191.

[32] Zhang H, Benoit H, Gauthier D, Degrève J, Baeyens J, López IP, et al. Particle circulation loops in solar energy capture and storage: gas-solid flow and heat transfer considerations. Appl Energy 2016;161:206–24. https://doi.org/10.1016/j.apenergy.2015.10.005.

[33] Benoit H, Spreafico L, Gauthier D, Flamant G. Review of heat transfer fluids in tube-receivers used in concentrating solar thermal systems: properties and heat transfer coefficients. Renew Sustain Energy Rev 2016;55:298–315. https://doi.org/10.1016/j.rser.2015.10.059.

[34] Ho C, Christian J, Gill D, Moya A, Jeter S, Abdel-Khalik S, et al. Technology advancements for next generation falling particle receivers. Energy Procedia 2014;49:398–407. https://doi.org/10.1016/j.egypro.2014.03.043.

[35] Flamant G, Gauthier D, Benoit H, Sans J-L, Garcia R, Boissière B, et al. Dense suspension of solid particles as a new heat transfer fluid for concentrated solar thermal plants: on-sun proof of concept. Chem Eng Sci 2013;102:567–76. https://doi.org/10.1016/j.ces.2013.08.051.

[36] Flamant G, Gauthier D, Benoit H, Sans JL, Boissière B, Ansart R, et al. A new heat transfer fluid for concentrating solar systems: particle flow in tubes. Energy Procedia 2014;49:617–26. https://doi.org/10.1016/j.egypro.2014.03.067.

[37] Le Gal A, Grange B, Tessonneaud M, Perez A, Escape C, Sans JL, Flamant G. Thermal analysis of fluidized particle flows in a finned tube solar receiver. Sol Energy 2019;191:19–33. https://doi.org/10.1016/j.solener.2019.08.062.

[38] Reyes-Belmonte MA, Sebastián A, Spelling J, Romero M, González-Aguilar J. Annual performance of subcritical Rankine cycle coupled to an innovative particle receiver solar power plant. Renew Energy 2019;130:786–95. https://doi.org/10.1016/j.renene.2018.06.109.

[39] Valentin B, Siros F, Brau JF. Optimization of a decoupled combined cycle gas turbine integrated in a particle receiver solar power plant. AIP Conf Proc 2019;2126:140007. https://doi.org/10.1063/1.5117655.

[40] Reyes-Belmonte MA, Díaz E, Romero M, González-Aguilar J. Particles-based thermal energy storage systems for concentrated solar power. AIP Conf Proc 2018;2033:210013. https://doi.org/10.1063/1.5067215.

[41] Kang Q, Flamant G, Dewil R, Baeyens J, Zhang HL, Deng YM. Particles in a circulation loop for solar energy capture and storage. Particuology 2019;43:149–56. https://doi.org/10.1016/j.partic.2018.01.009.

[42] CSP2 project (concentrated solar power in particules European project) n.d. https://www.csp2-project.eu/. [Accessed 26 October 2020].

[43] Gueguen R, Grange B, Bataille F, Mer S, Flamant G. Shaping high efficiency, high temperature cavity tubular solar central receivers. Energies 2020;13:4803. https://doi.org/10.3390/en13184803.

[44] Zhang H, Benoit H, Perez-Lopèz I, Flamant G, Tan T, Baeyens J. High-efficiency solar power towers using particle suspensions as heat carrier in the receiver and in the thermal energy storage. Renew Energy 2017;111:438–46. https://doi.org/10.1016/j.renene.2017.03.101.

[45] Li X, Kong W, Wang Z, Chang C, Bai F. Thermal model and thermodynamic performance of molten salt cavity receiver. Renew Energy 2010;35:981–8. https://doi.org/10.1016/j.renene.2009.11.017.

[46] Sánchez-Orgaz S, Medina A, Calvo Hernández A. Recuperative solar-driven multi-step gas turbine power plants. Energy Convers Manag 2013;67:171–8. https://doi.org/10.1016/j.enconman.2012.11.006.

[47] Ho CK, Iverson BD. Review of high-temperature central receiver designs for concentrating solar power. Renew Sustain Energy Rev 2014;29:835–46. https://doi.org/10.1016/j.rser.2013.08.099.

[48] Reyes-Belmonte MA, Gómez-García F, González-Aguilar J, Romero M, Benoit H, Flamant G. Heat exchanger modelling in central receiver solar power plant using dense particle suspension. AIP Conf Proc 2017;1850:030042. https://doi.org/10.1063/1.4984385.

[49] Reyes-Belmonte MA, Romero M, González-aguilar J. Integrated solar combined cycle using particles as heat transfer fluid and thermal energy storage medium for flexible electricity dispatch. AIP Conf Proc 2020;2303:130006. https://doi.org/10.1063/5.0029297.

[50] Schröder A, Kunz F, Meiss J, Mendelevitch R. Current and prospective costs of electricity generation until 2050. DIW Data D; 2013.

[51] Report C. Cost and performance data for power generation technologies. Prep Natl Renew Energy Lab; 2012.

[52] Wagner MJ, Wendelin T. SolarPILOT: a power tower solar field layout and characterization tool. Sol Energy 2018;171:185–96. https://doi.org/10.1016/j.solener.2018.06.063.

[53] Wendelin T. Soltrace: a new optical modeling tool for concentrating solar optics. Int Sol Energy Conf 2003:253–60. https://doi.org/10.1115/ISEC2003-44090.

[54] Schwarzbözl P. A TRNSYS model library for solar thermal electric components (STEC) reference manual release 3.0. Dtsch zent für luft und raumfahrt eV D-51170 köln, ger. http://www.trnsys.com/tess-libraries/index.html. [Accessed 2 September 2020].

[55] METEONORM. Handbook part II : theory global meteorological database

version 7 software and data for engineers, planers and education. Handb Part II Theory; 2019.
[56] Balz M, Göcke V, Keck T, Von Reeken F, Weinrebe G, Wöhrbach M. Stellio - development, construction and testing of a smart heliostat. AIP Conf Proc 2016;1734:020002. https://doi.org/10.1063/1.4949026.
[57] Gallo A, Spelling J, Romero M, González-Aguilar J. Preliminary design and performance analysis of a multi-megawatt scale dense particle suspension receiver. Energy Procedia 2015;69:388–97. https://doi.org/10.1016/j.egypro.2015.03.045.
[58] Peruchena CMF, Ramírez L, Silva M, Lara V, Bermejo D, Gastón M, et al. A methodology for calculating percentile values of annual direct normal solar irradiation series. AIP Conf Proc 2016;1734:150005. https://doi.org/10.1063/1.4949237.
[59] SunEarthTools.com n.d. https://www.sunearthtools.com/dp/tools/pos_sun.php?lang=it#annual. [Accessed 2 September 2020].
[60] Masaki MS, Zhang L, Xia X. A comparative study on the cost-effective belt conveyors for bulk material handling. Energy Procedia 2017;142:2754–60. https://doi.org/10.1016/j.egypro.2017.12.221.
[61] Roberts AW. Economic analysis in the optimisation of belt conveyor systems. Proc Beltcon 1981;1:1–33. Conf 1981, http://www.saimh.co.za/beltcon/beltcon1/paper11.html. [Accessed 2 September 2020].
[62] Isles J. Gas turbine world, vol. 33. Southport, CT: USA Pequot Publ Inc; 2018. Handbook, https://gasturbineworld.com/shop/annual-handbook/2018-handbook-volume-33/. [Accessed 2 September 2020]. 2018.
[63] Roosen P, Uhlenbruck S, Lucas K. Pareto optimization of a combined cycle power system as a decision support tool for trading off investment vs. operating costs. Int J Therm Sci 2003;42:553–60. https://doi.org/10.1016/S1290-0729(03)00021-8.
[64] Silveira JL, Tuna CE. Thermoeconomic analysis method for optimization of combined heat and power systems. Part II. Prog Energy Combust Sci 2003;29:673–8. https://doi.org/10.1016/j.pecs.2003.06.001.
[65] Ilett T, Lawn CJ. Thermodynamic and economic analysis of advanced and externally fired gas turbine cycles. Proc Inst Mech Eng Part A J Power Energy 2010;224:901–15. https://doi.org/10.1243/09576509JPE967.
[66] Thermoflow-Inc.. GT PRO – gas - turbine combined cycle design program to create cycle heat balance and physical equipment needed to realize it. 2018. http://www.thermoflow.com/combinedcycle_GTP.html. [Accessed 2 September 2020].
[67] Turchi CS, Boyd M, Kesseli D, Kurup P, Mehos M, Neises T, et al. reportCSP systems analysis - final project report CSP systems analysis - final project report 2019.
[68] Zaversky F, Les I, Sánchez M, Valentin B, Brau J-F, Siros F, et al. Techno-economic optimization and benchmarking of a solar-only powered combined cycle with high-temperature TES upstream the gas turbine. IntechOpen: Green Energy Environ.; 2020. https://doi.org/10.5772/intechopen.90410.
[69] Ma Z, Glatzmaier GC, Mehos M. Development of solid particle thermal energy storage for concentrating solar power plants that use fluidized bed technology. Energy Procedia 2014;49:898–907. https://doi.org/10.1016/j.egypro.2014.03.097.
[70] Spelling J, Gallo A, Romero M, González-Aguilar J. A high-efficiency solar thermal power plant using a dense particle suspension as the heat transfer fluid. Energy Procedia 2015;69:1160–70. https://doi.org/10.1016/j.egypro.2015.03.191.
[71] Ho Clifford K. A review of high-temperature particle receivers for concentrating solar power. Appl Therm Eng 2016;109:958–69.
[72] Zhao L, Wang W, Zhu L, Liu Y, Dubios A. Economic analysis of solar energy development in North Africa. Glob Energy Interconnect 2018;1:53–62. https://doi.org/10.14171/j.2096-5117.gei.2018.01.007.